Inorganic Chemistry

Article

pubs.acs.org/IC

Solution-Chemical Route to Generalized Synthesis of Metal Germanate Nanowires with Room-Temperature, Light-Driven Hydrogenation Activity of CO_2 into Renewable Hydrocarbon Fuels

Qi Liu,[†,‡] Yong Zhou,*[,§,⊥] Wenguang Tu,[∥] Shicheng Yan,[†] and Zhigang Zou*[,⊥]

[§]Key Laboratory of Modern Acoustics, MOE, Institute of Acoustics, School of Physics, [⊥]National Laboratory of Solid State Microstructures, School of Physics, Ecomaterials and Renewable Energy Research Center (ERERC), [†]ERERC, Department of Materials Science and Engineering, and [∥]ERERC, School of Physics, Nanjing University, Nanjing 210093, People's Republic of China

[‡]School of Mechanical and Automotive Engineering, Anhui Polytechnic University, Wuhu 241000, People's Republic of China

S *Supporting Information*

ABSTRACT: A facile solution-chemical route was developed for the generalized preparation of a family of highly uniform metal germanate nanowires on a large scale. This route is based on the use of hydrazine monohydrate/H_2O as a mixed solvent under solvothermal conditions. Hydrazine has multiple effects on the generation of the nanowires: as an alkali solvent, a coordination agent, and crystal anisotropic growth director. Different-percentage cobalt-doped $Cd_2Ge_2O_6$ nanowires were also successfully obtained through the addition of $Co(OAc)_2{\cdot}4H_2O$ to the initial reaction mixture for future investigation of the magnetic properties of these nanowires. The considerably negative conduction band level of the $Cd_2Ge_2O_6$ nanowire offers a high driving force for photogenerated electron transfer to CO_2 under UV−vis illumination, which facilitates CO_2 photocatalytic reduction to a renewable hydrocarbon fuel in the presence of water vapor at room temperature.

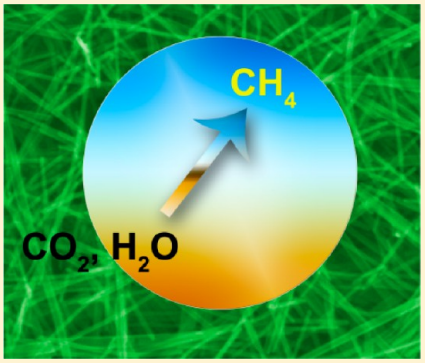

INTRODUCTION

One-dimensional (1D) functional oxide nanostructures, such as nanotubes, nanowires, and nanobelts, have attracted much interest because of their unique chemical, electronic, and optical properties.[1] 1D ternary nanostructures are technologically important because their properties, and hence functionalities, can be efficiently tuned by changing the ratio of the component elements. Compared with the extensive research on binary oxide materials, investigations on 1D ternary nanostructures are relatively limited because of the difficulties inherent in their preparations. Among ternary functional oxide, metal germinates are unique compounds with extended structures consisting of GeO_4 tetrahedra, GeO_5 trigonal bipyramids, and GeO_6 octahedra,[2] which have attracted intensive attention in the areas of photocatalysis, adsorption, ion exchange, humidity sensors, and high-energy laser systems. The corresponding ternary germanate 1D nanomaterials, such as $In_2Ge_2O_7$ nanowires,[3] nanobelts,[3−5] and nanotubes[6,7] and Zn_2GeO_4 nanowires,[8−11] have already been prepared via vapor−solid mechanisms. Soft surfactant-assistant, solution-based processes can be easily expanded to the industrial scale at low temperature for the synthesis of $CuGeO_3$[12] and Bi_2GeO_5 nanobelts,[13] $Ca_5Ge_2O_9$,[14] and $PbGeO_3$[15] and Zn_2GeO_4 nanowires.[16−18] Therefore, it is essentially significant to develop a general route for the synthesis of metal germanate 1D nanostructures.

In this paper, we report a facile solution-chemical pathway to generalized synthesis of a family of metal germanate nanowires including, but not limited to, $Cd_2Ge_2O_6$, Co-doped $Cd_2Ge_2O_6$, Zn_2GeO_4, and $PbGeO_3$ on a large scale. This route is based on the use of hydrazine monohydrate in multiple roles, i.e., as an alkali solvent, a coordination agent, and a anisotropic crystal growth director, for the synthesis of the nanowires under solvothermal conditions. The considerably negative conduction band level of the $Cd_2Ge_2O_6$ nanowire offers a high driving force for photogenerated electron transfer to CO_2 under UV−vis illumination, which facilitates CO_2 photocatalytic reduction into renewable hydrocarbon fuel in the presence of water vapor at room temperature.

EXPERIMENTAL SECTION

Preparation of the 1D Metal Germanate Nanostructures. All of the chemicals were of analytical grade and were used as received without further purification. The germanates were synthesized in a binary hydrazine hydrate/water solvent system using a solvothermal route. The typical preparation procedure of the $Cd_2Ge_2O_6$ nanowire was as follows: 0.105 g of GeO_2 (1 mmol) and 0.267 g of $Cd(OAc)_2{\cdot}2H_2O$ (1 mmol) were added to 15 mL of solvents, which include 10 mL of H_2O and 5 mL of hydrazine monohydrate. The mixture was stirred for 40 min and then transferred to a stainless steel, Teflon-lined autoclave of 25 mL inner volume. Solvothermal synthesis was performed under an autogenerated pressure at 180 °C for 12 h in an electric oven, followed by cooling naturally to room temperature. The product was collected by centrifugation, washed thoroughly with

Received: September 10, 2013
Published: December 19, 2013

   dx.doi.org/10.1021/ic402292a | *Inorg. Chem.* 2014, 53, 359−364

deionized water and alcohol several times, and then dried at 60 °C for 12 h. A white $Cd_2Ge_2O_6$ powder was finally obtained. Similarly, in the case of synthesis of the Zn_2GeO_4 and $PbGeO_3$ nanowires, $Zn(OAc)_2 \cdot 2H_2O$ and $Pb(OAc)_2 \cdot 2H_2O$ were used as metal resources. Synthesis of different-percentage Co-doped $Cd_2Ge_2O_6$ nanowires was obtained through the addition of $Co(OAc)_2 \cdot 4H_2O$ to the initial reaction mixture. The concentration of Cd^{2+} was reduced to keep the total initial concentration of metal ions constant in doping. The doping content of Co was obtained by theoretical calculation, denoting the Co atomic percentage of the total elements (Co and Cd) contained in the acetate precursors.

Characterization. The crystallographic phase of these as-prepared products was determined by X-ray diffraction (XRD; Rigaku Ultima III, Japan) using Cu Kα radiation (λ = 0.154178 nm) at 40 kV and 40 mA. The XRD patterns were obtained over a scanning range of 10–80° at room temperature with a scan rate of 10° min^{-1}. The morphology of the powders was examined by field-emission scanning electron microscopy (FESEM; FEI NOVA NANOSEM 230). Transmission electron microscopy (TEM) and high-resolution TEM (HRTEM) images were obtained on a JEOL JEM-2100 microscope with a LaB_6 filament and an accelerating voltage of 200 kV. The chemical compositions were analyzed with X-ray photoelectron spectroscopy (XPS; K-Alpha, Thermo Fisher Scientific). The XPS spectrum was calibrated with respect to the binding energy of the adventitious C 1s peak at 284.8 eV. The UV–vis diffuse-reflectance spectrum was recorded with a UV–vis spectrophotometer (UV-2550, Shimadzu) at room temperature and transformed to the absorption spectrum according to the Kubelka–Munk relationship. The specific surface area of the samples was measured by nitrogen sorption at 77 K on a surface area and porosity analyzer (Micromeritics TriStar 3000) and calculated by the Brunauer–Emmett–Teller (BET) method. CO_2 adsorption isotherms were measured at 273 K on an automatic volumetric adsorption apparatus (Micromertics ASAP 2010).

Photocatalytic Conversion of CO_2. Before photocatalytic reaction, the catalysts were degassed at 200 °C for 12 h under vacuum to remove the adsorption materials. CO_2 photoreduction can be carried out at room temperature. Typically, 0.1 g of powdered photocatalyst was uniformly placed at the bottom of a Pyrex glass cell with an area of 4.2 cm^2. The reaction was in a gastight system with a volume of about 230 mL. The reaction setup was vacuum-treated several times, and then high-purity CO_2 gas was introduced into the reaction to achieve ambient pressure. A total of 0.4 mL of deionized water was injected into the system as a reducer. After adsorption of CO_2 reached equilibrium in the dark, light photoirradiation was performed using a UV-enhanced 300 W xenon arc lamp with a water filter. A gas pump was used to accelerate gas diffusion. The concentration of the product in the tube was withdrawn with a gastight syringe and detected by a gas chromatograph (Shimadzu, GC-14B with a flame ionization detector, Japan). The quantum yield was measured by inserting a 320-nm-band-pass filter in front of the reaction cell to supply irradiant light with a wavelength of 320 ± 15 nm.

RESULTS AND DISCUSSION

The XRD patterns show that all of the diffraction peaks of the different products could be readily indexed to $Cd_2Ge_2O_6$ (monoclinic) with lattice constants of a = 10.184 Å, b = 9.652 Å, c = 5.377 Å, $\alpha = \beta$ = 90°, and γ = 120°, Zn_2GeO_4 (rhombohedral phase) with lattice constants of $a = b$ = 1.423 nm, c = 0.953 nm, $\alpha = \beta$ = 90°, and γ = 120°, and $PbGeO_3$ (hexagonal phase) with lattice constants of $a = b$ = 1.57 nm, c = 0.724 nm, $\alpha = \beta$ = 90°, and γ = 120° (Figure 1), which are in good agreement with literature values (JCPDS nos. 43-0468, 11-0687, and 38-1035).

The typical FESEM image of the $Cd_2Ge_2O_6$ nanowire shows that the product mainly consists of high-yield, uniform, wirelike nanostructures (Figure 2 and Figure S1 in the Supporting Information, SI). The nanowire possesses a smooth and clean

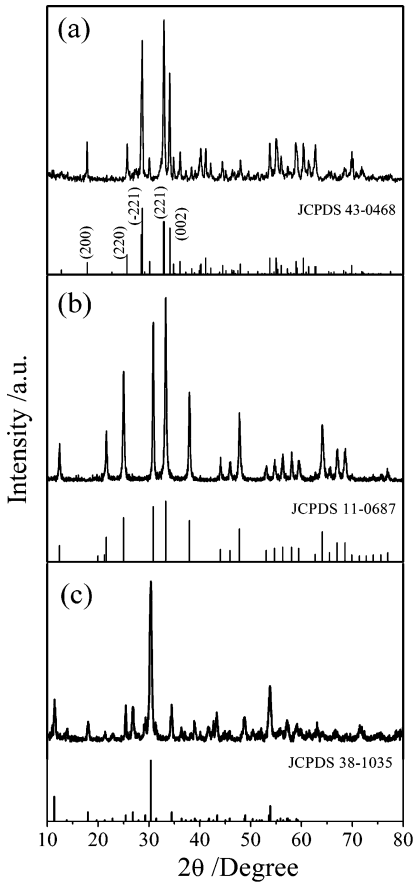

Figure 1. XRD patterns of (a) $Cd_2Ge_2O_6$, (b) Zn_2GeO_4, and (c) $PbGeO_3$ nanowires.

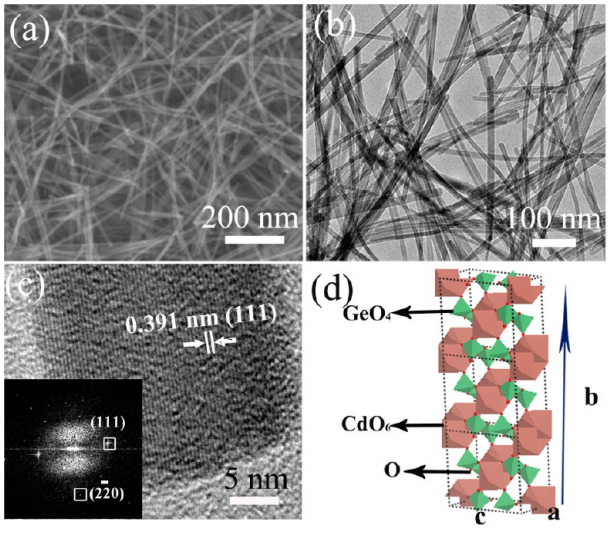

Figure 2. (a) FESEM, (b) TEM, and (c) HRTEM images of $Cd_2Ge_2O_6$ nanowires formed with a volume ratio of 1:2 $N_2H_4 \cdot H_2O$/H_2O for 12 h. The inset of part c shows the corresponding FFT pattern. (d) Molecular structure model of $Cd_2Ge_2O_6$.

surface without any adhesive particles and exhibits narrow-diameter distributions with typical diameters of 15 ± 5 nm and lengths of up to tens of micrometers. A large number of nanowires intertwist with each other to form networks, indicative of the flexibility of the nanowire. The TEM image further demonstrates a wirelike architecture with diameters of

dx.doi.org/10.1021/ic402292a | Inorg. Chem. 2014, 53, 359–364

10−20 nm. The typical HRTEM image shows crystal lattice fringes with $d_{(111)}$ = 0.391 nm, demonstrating a {110} growth direction of the $Cd_2Ge_2O_6$ nanowire (Figure 2c), well consistent with the corresponding fast Fourier transform (FFT) pattern. Similarly, uniform Zn_2GeO_4 and $PbGeO_3$ nanowires were also obtained, as depicted in the gallery pictures (Figure 3). The Zn_2GeO_4 nanowire is of 20−50 nm

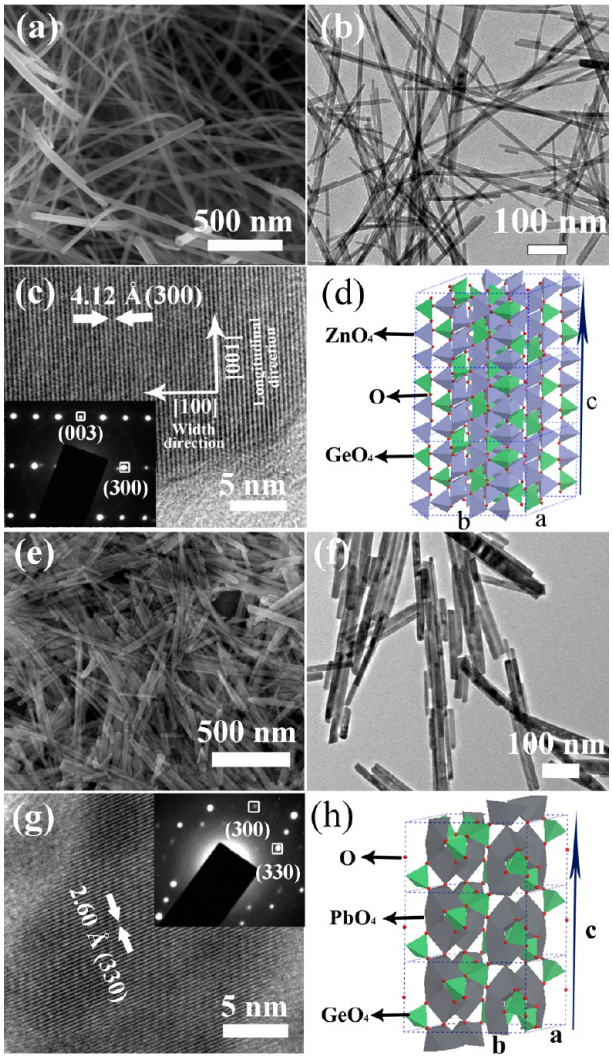

Figure 3. (a) FESEM, (b) TEM, and (c) HRTEM images of the Zn_2GeO_4 nanowire. The inset of part c shows the SAED pattern. (d) Molecular structure model of Zn_2GeO_4. (e) FESEM, (f) TEM, and (g) HRTEM images of the $PbGeO_3$ nanowire. The inset of part g shows the SAED pattern. (h) Molecular structure model of $PbGeO_3$.

diameters and lengths up to several tens of micrometers. The selected-area electron diffraction (SAED) pattern indicates that the nanowire is a uniform single crystal with the longitudinal direction along [001] and the width direction along [100]. The resulting $PbGeO_3$ is composed of a large amount of relatively short nanowire with 20−50 nm diameters and 200−600 nm lengths, growing along the [100] direction.

The XPS spectrum shows two strong peaks taken for the Cd region at 404.68 eV [$Cd(3d_{5/2})$] and 411.58 eV [$Cd(3d_{3/2})$] (Figure S2 in the SI, left panel), inferring the existence of Cd in the Cd^{2+} oxidation state. The Ge 3d peak centered at 31.88 eV is consistent with that of Ge^{IV} (31.8 eV) in germinate rather than Ge (32.5 eV) in GeO_2.[19] The O 1s peak centered at 530.18 eV is assignable to the lattice O and not to the hydroxyl groups located at 531.4 eV, indicating that the nanowires contain no −OH group.[20,21] Similar XPS spectra also demonstrate the presence of Zn, Ge, and O of the Zn_2GeO_4 nanowire and Pb, Ge, and O of the $PbGeO_3$ nanowire (Figure S2 in the SI, middle and right panels, respectively).

The hydrazine is indispensable for 1D anisotropic growth of the metal germanate nanowires. Employment of pure water as a single solvent produced short and thick $Cd_2Ge_2O_6$ nanowires (Figure 4a). Increasing the volume of hydrazine monohydrate

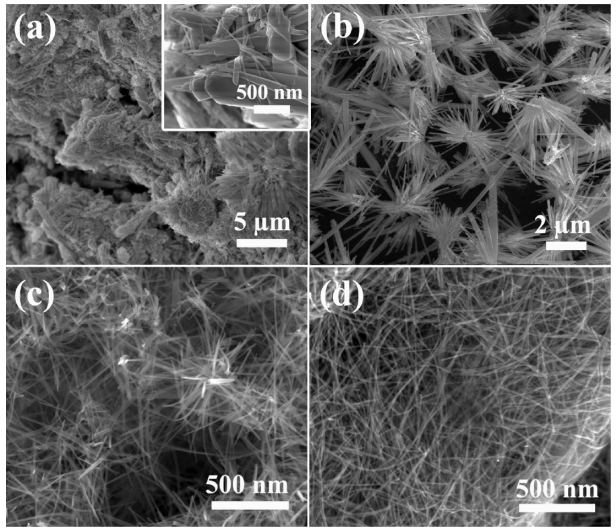

Figure 4. FESEM images of $Cd_2Ge_2O_6$ produced with different volumes of $N_2H_4{\cdot}H_2O$: (a) 0 mL; (b) 1 mL; (c) 3 mL; (d) 5 mL.

to 1 mL leads to monodisperse $Cd_2Ge_2O_6$ bundles, which consist of well-aligned nanorods with ∼60 nm diameter oriented toward its center and radically projecting out at one end (Figure 4b). Abundant $Cd_2Ge_2O_6$ nanowires were harvested as the volume of $N_2H_4{\cdot}H_2O$ was increased to 3 mL (Figure 4c). Further increasing the volume to 5 mL, the nanowires grow longer with more perfect shape and intertwist with each other to form networks (Figure 4d).

The time-resolved XRD patterns and corresponding FESEM images enable us to trace the formation evolution of the $Cd_2Ge_2O_6$ nanowires (Figure 5). The feeble diffraction peaks of the product obtained for 1 h were attributed to the cubic $NH_4H_3Ge_2O_6$ (Figure 5a,e), and the phase and morphology are the same as those of the product employing GeO_2 as a single reactant (Figure S3 in the SI for the XRD pattern and FESEM image). Very small aggregate protofibrils of monoclinic $Cd_2Ge_2O_6$ were obtained after a solvothermal reaction time of 4 h (Figure 5b,f). After a reaction time of 8 h, highly uniform nanowires with diameters of 10−20 nm and lengths of several hundreds of nanometers of the monoclinic $Cd_2Ge_2O_6$ crystal became dominate (Figure 5c,g). With elongation of the reaction to 12 h, all of the diffraction peaks of the products could be readily indexed to the monoclinic $Cd_2Ge_2O_6$ crystal. The nanowire continuously grew along their length axis with constant diameter (Figure 5d,h).

$N_2H_4{\cdot}H_2O$ is an excellent alkaline solvent that could act as a reducing reagent, coordination, and linking molecule in the formation of many micro/nanostructures. In the present case, the hydrazine molecules take on multiple roles in the formation

dx.doi.org/10.1021/ic402292a | Inorg. Chem. 2014, 53, 359−364

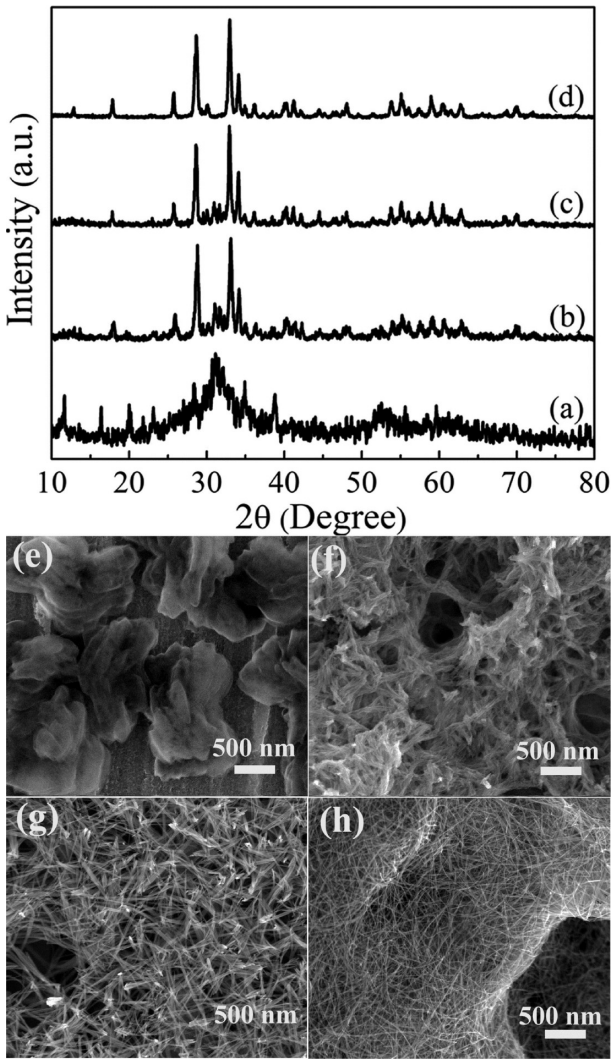

Figure 5. XRD patterns and corresponding FESEM images of the intermediates during formation of the $Cd_2Ge_2O_6$ nanowire with a volume ratio of 1:2 $N_2H_4{\cdot}H_2O/H_2O$ at different solvothermal reaction times: (a and e) 1 h; (b and f) 4 h; (c and g) 8 h; (d and h) 12 h.

of metal germanate nanowires. At the beginning of the reaction, $N_2H_4{\cdot}H_2O$ molecules in the starting solution serve as the coordinating agent using a gauche conformation to chelate with Cd^{2+} to form a complex ion, $[Cd(N_2H_4)_2]^{2+}$. With the solvothermal process, N_2H_4 then acts as an alkali agent, decomposing into N_2, NH_3, and H_2. It allows generation of an alkaline environment, in which GeO_2 hydrolyzes to form $NH_4H_3Ge_2O_6$. $[Cd(N_2H_4)_2]^{2+}$ was also slowly decomposed and released free Cd^{2+} cations and subsequently reacted with $NH_4H_3Ge_2O_6$ to form $Cd_2Ge_2O_6$. Such a slow decomposition is favorable for the preferentially anisotropic growth of the nanowire. The possible reactions are thought to occur in solution as follows:

$$Cd(CH_3COO)_2 + 2N_2H_4 \rightarrow [Cd(N_2H_4)_2]^{2+} + 2CH_3COO^- \quad (1)$$

$$2N_2H_4 \rightarrow N_2\uparrow + 3NH_3 + H_2\uparrow \quad (2)$$

$$2GeO_2 + 2H_2O + NH_3 \rightarrow NH_4H_3Ge_2O_6 \quad (3)$$

$$[Cd(N_2H_4)_2]^{2+} \rightarrow Cd^{2+} + 2N_2H_4 \quad (4)$$

$$2Cd^{2+} + NH_4H_3Ge_2O_6 \rightarrow Cd_2Ge_2O_6 + NH_3\uparrow + 4H^+ \quad (5)$$

Substitution of ethylenediamine (en, $NH_2CH_2CH_2NH_2$) for $N_2H_4{\cdot}H_2O$ results in a clear solution without any precipitation, which is due to the much stronger coordination ability of en to Cd^{2+} than N_2H_4 to form the highly stable $[Cd(en)_2]^{2+}$ complex that prevents the release of free Cd^{2+} for the heterogeneous reaction with $NH_4H_3Ge_2O_6$. Meanwhile, a N_2H_4 molecule containing two N atoms, being a strong Lewis base with lone pairs of electrons, can saturate the Cd dangling bonds and selectively bind or link to some specific panels of forming $Cd_2Ge_2O_6$ nuclei to control the velocity and direction of crystal growth.[22,23] The control ability of the crystal morphology of hydrazine was also evidenced with the formation of hexagonal $Cd(OH)_2$ nanoplates with highly preferential growth along {001} with $Cd(OAc)_2$ as a single reactant in the solvent of 10 mL of H_2O and 5 mL of $N_2H_4{\cdot}H_2O$ (see Figure S4 in the SI for the XRD pattern and corresponding FESEM image).

Magnetic semiconductors such as Co-doped TiO_2 are semiconductor materials that exhibit both ferromagnetism (or a similar response) and useful semiconductor properties. If implemented in devices, these materials could provide a new type of control of conduction.[24−26] Different-percentage Co-doped $Cd_2Ge_2O_6$ nanowires were successfully obtained through the addition of $Co(OAc)_2{\cdot}4H_2O$ to the initial reaction mixture. The Co concentration is a theoretical value, which is calculated from the Co atomic percentage of the total elements (Co and Cd) contained in the acetate precursors. The XRD patterns of all of the Co-doped $Cd_2Ge_2O_6$ nanowires are very similar to the monoclinic $Cd_2Ge_2O_6$ (Figure 6a−e). A careful comparison of the diffraction peaks in the range of 2θ = 32−35° shows that

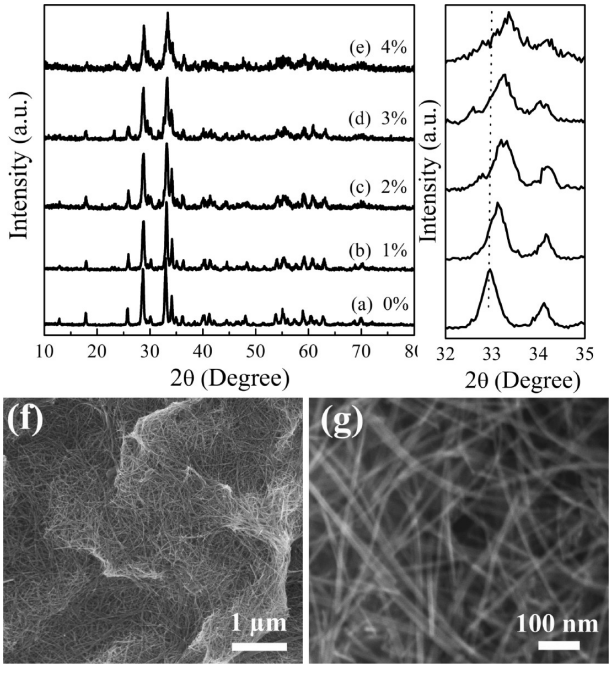

Figure 6. (a−e) XRD patterns of the Co-doped $Cd_2Ge_2O_6$ with different cobalt percentages in the reaction precursors. The right panel shows diffraction peak positions of the (110) plane in the range of 2θ = 32−35°. (f and g) FESEM images of Co-doped $Cd_2Ge_2O_6$ nanowires (2% Co as the example).

dx.doi.org/10.1021/ic402292a | Inorg. Chem. 2014, 53, 359−364

the peak position of Co-doped $Cd_2Ge_2O_6$ samples slightly shifted toward a higher 2θ value, originating from an ionic radius of Co^{2+} (0.074 nm) smaller than that of Cd^{2+} (0.097 nm). The SEM image shows that the Co-doped $Cd_2Ge_2O_6$ nanowire maintains a highly uniform 1D structure (Figure 6f,g).

The UV−vis absorption spectra show that the absorption threshold of the pristine $Cd_2Ge_2O_6$ nanowire is located at about 320 nm (Figure S5 in the SI), corresponding to a band gap of ~3.9 eV, in good agreement with the reported value.[27] The presence of cobalt doping ions caused significant absorption shifts in the visible region with the absorption edge at around 430 nm (2.9 eV) compared to that of $Cd_2Ge_2O_6$. A new absorption peak at ~400 nm arises in Co-doped $Cd_2Ge_2O_6$, which may result from charge transfer and d−d transitions.[28] The Co 2p peak at 781.4 eV indicated that the Co moiety exists as the state of Co^{2+} in the doped $Cd_2Ge_2O_6$ (Figure S2d in the SI). The magnetic properties of these semiconductor nanowires are currently investigated.

The use of solar energy to chemically reduce CO_2 to higher-energy compounds such as methanol or methane offers an ideal way to address both environment and energy crisis problems.

Considerable semiconductor photocatalysts have been explored to develop reliable, efficient photocatalysts for the reduction of CO_2, such as TiO_2,[29−31] $W_{18}O_{49}$,[32] $ZnGa_2O_4$,[33,34] Zn_2GeO_4,[18] etc. Here we develop the $Cd_2Ge_2O_6$ nanowires for the highly photocatalytic activity of CO_2 conversion into renewable hydrocarbon fuel in the presence of vapor H_2O performed at room temperature. Generally, CO_2 in the presence of water vapor could be photoreduced to CH_4 using a wide-band-gap semiconductor as the photocatalyst such as TiO_2. The photogenerated holes in the valence band oxidize water to generate H ions via the reaction $H_2O \rightarrow {}^1/_2O_2 + 2H^+ + 2e^-$ (E°_{redox} = 0.82 V vs NHE), and the photogenerated electrons in the conduction band reduce CO_2 to CH_4 via the reaction $CO_2 + 8e^- + 8H^+ \rightarrow CH_4 + 2H_2O$ (E°_{redox} = −0.24 V vs NHE).[35] The electronic structure of $Cd_2Ge_2O_6$ has been calculated using density functional theory. The top of the valence band of $Cd_2Ge_2O_6$ is mainly composed of the O 2p levels, and the bottom of the conduction band is the hybridized orbital of the Ge 4s4p and Cd 5s5p states.[27] The band gap of the $Cd_2Ge_2O_6$ nanowire is determined based on the UV−vis absorption spectrum to be around 3.9 eV (Figure S5 in the SI). The positions of the corresponding conduction and valence bands could be determined by the following equation:[36,37]

$$E_{CB} = X - E_c - 0.5E_g$$

where E_c is the energy of free electrons on the hydrogen scale (4.5 eV), X is the electronegativity of the semiconductor, and E_g is the band-gap energy of the semiconductor. The edge of the valence band (E_{VB}) of the $Cd_2Ge_2O_6$ nanowire is determined to be 2.71 V (vs NHE), more positive than that of $E^\circ(H_2O/H^+)$ (0.82 V vs NHE), and the edge of the conduction band is estimated as −1.19 V (vs NHE) and is more negative than that of $E^\circ(CO_2/CH_4)$ (−0.24 V vs NHE). In photocatalytic CO_2 reduction studies, the focus lies mostly on the reduction side, which involves multiple electron transfers. This reflects the fact that CO_2 reduction is a more complex and difficult process to realize than the generation of hydrogen from water.[29]

The considerably negative conduction band level of the $Cd_2Ge_2O_6$ nanowire offers a high driving force for photogenerated electron transfer to CO_2 under UV−vis illumination, which facilitates CO_2 photocatalytic reduction into renewable hydrocarbon fuel in the presence of water vapor at room temperature (Figure S6 in the SI). Figure 7 shows the

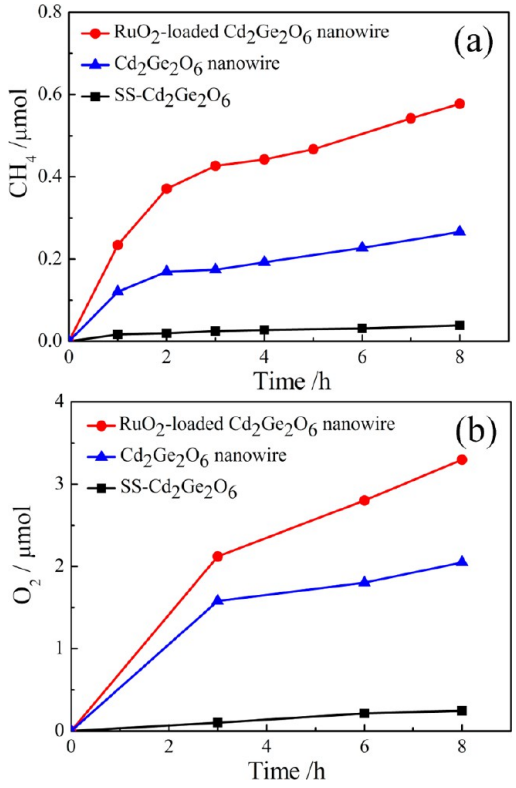

Figure 7. Generation of the gaseous products over various $Cd_2Ge_2O_6$ during CO_2 photoreduction under UV−vis light irradiation: (a) CH_4; (b) O_2.

photocatalytic activity of CO_2 reduction over $Cd_2Ge_2O_6$ nanowires along with bulky $Cd_2Ge_2O_6$ obtained by the solid-state reaction (SSR) of $Cd(OAc)_2{\cdot}2H_2O$ and GeO_2 at 1100 °C for 16 h. Relative to the trace amount generation of CH_4 and O_2 over the SSR $Cd_2Ge_2O_6$, the yield of the $Cd_2Ge_2O_6$ nanowires increased with the photocatalytic time, and the total yield of CH_4 and O_2 obtained after 8 h of continuous irradiation is 0.266 and 2.05 μmol, corresponding to approximately 0.033 μmol h^{-1} CH_4 formation rate and 0.256 μmol h^{-1} O_2 generation rate. The generation rate ratio of CH_4 to O_2 over $Cd_2Ge_2O_6$ nanowires is 1:7.76, smaller than the theoretical mole ratio (1:2 CH_4/O_2 based on $CO_2 + 2H_2O \rightarrow CH_4 + 2O_2$). The stoichiometric imbalance for CH_4 to O_2 suggests that other reduction products besides CH_4 form.[38] For instance, a low content of CO can be detected in the gaseous products.[39] The reduction experiment of CO_2 preformed in the dark or in the absence of a photocatalyst shows no appearance of CH_4, proving that the reduction reaction of CO_2 is driven by light under the photocatalyst. The higher photocatalytic activity of the $Cd_2Ge_2O_6$ nanowires toward reduction of CO_2 relative to that of SSR-$Cd_2Ge_2O_6$ can be attributed to their higher specific surface area because of the special 1D morphology. The 1D morphology of the $Cd_2Ge_2O_6$ nanowire offers a high BET surface area of 23.8 m^2 g^{-1}, over 25 times larger than 0.94 m^2 g^{-1} for SSR-$Cd_2Ge_2O_6$, which renders these nanowires more reactive sites and higher CO_2 adsorption capacity (Figure S7 in the SI) to improve the photocatalytic activity. The photocatalytic activity of the photocatalyst could be significantly

dx.doi.org/10.1021/ic402292a | Inorg. Chem. 2014, 53, 359−364

enhanced by loading specific noble metals (e.g., Pt and Rh) or metal oxides (e.g., NiO and RuO_2) as cocatalysts. The generation rate of CH_4 over a 1 wt % RuO_2-loaded $Cd_2Ge_2O_6$ nanowire was determined to be 0.072 μmol h^{-1}, about 2.2 times higher than the unloaded ones, because of the improved separation of photogenerated electron−hole pairs with cocatalyst RuO_2 as a hole sink. The quantum yield was calculated according to the equation[40]

$$E_Q = [N(CH_4) \times 8]/N(\text{photons}) \times 100\%$$

in which $N(CH_4)$ and N(photons) signify the molecular number of generated CH_4 in unit time and the number of incident photons in unit time, respectively. The apparent quantum yield of CH_4 evolution of these catalysts at a wavelength of 320 ± 15 nm was measured to be 0.04% for $Cd_2Ge_2O_6$ photocatalyst and 0.06% for RuO_2-loaded $Cd_2Ge_2O_6$ photocatalyst. The photoconversion rate of CO_2 may be further enhanced through nonmetal doping to level up the valence band of the $Cd_2Ge_2O_6$ nanowire in order to narrow the band gap to extend light absorption to the red.

CONCLUSION

In summary, a family of highly uniform metal germanate nanowires were synthesized in a hydrazine monohydrate/H_2O binary solvent system. Hydrazine plays multiple roles in the generation of nanowires such as an alkali solvent, a coordination agent, and a crystal anisotropic growth director. The considerably negative conduction band level of the $Cd_2Ge_2O_6$ nanowire offers a high driving force for photogenerated electron transfer to CO_2 under UV−vis illumination, which facilitates CO_2 photocatalytic reduction into renewable hydrocarbon fuel in the presence of water vapor at room temperature.

ASSOCIATED CONTENT

Supporting Information

SEM images, XPS spectra, XRD patterns, UV−vis absorption spectra, and CO_2 adsorption isotherms of the prepared materials. This material is available free of charge via the Internet at http://pubs.acs.org.

AUTHOR INFORMATION

Corresponding Authors

*E-mail: zhouyong1999@nju.edu.cn. Tel: +86 25 8362 1372.
*E-mail: zgzou@nju.edu.cn. Tel: +86 25 8362 1372.

Notes

The authors declare no competing financial interest.

ACKNOWLEDGMENTS

This work was supported by 973 Program (Grants 2014CB239302, 2011CB933303, and 2013CB632404), NSFC (Grants 51302001 and 21301002), National Science Foundation of Jiangsu Province (Grants BK2012015 and BK20130053), and College Postgraduate Research Innovation Project of Jiangsu Province (Grant CXZZ13 0033).

REFERENCES

(1) Xia, Y. N.; Yang, P. D.; Sun, Y. G.; Wu, Y. Y.; Mayers, B.; Gates, B.; Yin, Y. D.; Kim, F.; Yan, Y. Q. *Adv. Mater.* **2003**, *15*, 353.
(2) Li, H. L.; Eddaoudi, M.; Yaghi, O. M. *Angew. Chem., Int. Ed.* **1999**, *38*, 653.
(3) Yan, C. Y.; Singh, N.; Lee, P. S. *Cryst. Growth Des.* **2009**, *9*, 3697.
(4) Su, Y.; Li, S.; Xu, L.; Chen, Y. Q.; Zhou, Q. T.; Peng, B.; Yin, S.; Meng, X.; Liang, X. M.; Feng, Y. *Nanotechnology* **2006**, *17*, 6007.
(5) Li, L.; Lee, P. S.; Yan, C.; Zhai, T.; Fang, X.; Liao, M.; Koide, Y.; Bando, Y.; Golberg, D. *Adv. Mater.* **2010**, *22*, 5145.
(6) Zhan, J. H.; Bando, Y.; Hu, J. Q.; Yin, L. W.; Yuan, X. L.; Sekigitchi, T.; Golberg, D. *Angew. Chem., Int. Ed.* **2006**, *45*, 228.
(7) Yan, C. Y.; Zhang, T.; Lee, P. S. *Cryst. Growth Des.* **2008**, *8*, 3144.
(8) Yan, C. Y.; Singh, N.; Lee, P. S. *Appl. Phys. Lett.* **2010**, *96*, 053108.
(9) Yan, C. Y.; Lee, P. S. *J. Phys. Chem. C* **2009**, *113*, 14135.
(10) Li, C.; Bando, Y.; Liao, M. Y.; Koide, Y.; Golberg, D. *Appl. Phys. Lett.* **2010**, *97*, 161102.
(11) Hung, C. C.; Chang, M. P.; Ho, C. Y.; Yu, C. K.; Lin, W. T. *J. Electrochem. Soc.* **2010**, *157*, K80.
(12) Song, R. Q.; Xu, A. W.; Yu, S. H. *J. Am. Chem. Soc.* **2007**, *129*, 4152.
(13) Chen, R.; Bi, J.; Wu, L.; Li, Z.; Fu, X. *Cryst. Growth Des.* **2009**, *9*, 1775.
(14) Pei, L. Z.; Yang, Y.; Fan, C. G.; Yuan, C. Z.; Duan, T. K.; Zhang, Q.-F. *CrystEngComm* **2011**, *13*, 4658.
(15) Wang, N.; Ding, J.; Li, G.; Peng, H. *Cryst. Res. Technol.* **2010**, *45*, 316.
(16) Huang, J. H.; Ding, K. N.; Hou, Y. D.; Wang, X. C.; Fu, X. Z. *ChemSusChem* **2008**, *1*, 1011.
(17) Huang, J. H.; Wang, X. C.; Hou, Y. D.; Chen, X. F.; Wu, L.; Fu, X. Z. *Environ. Sci. Technol.* **2008**, *42*, 7387.
(18) Liu, Q.; Zhou, Y.; Kou, J.; Chen, X.; Tian, Z.; Gao, J.; Yan, S.; Zou, Z. *J. Am. Chem. Soc.* **2010**, *132*, 14385.
(19) Gao, Q. S.; Chen, P.; Zhang, Y. H.; Tang, Y. *Adv. Mater.* **2008**, *20*, 1837.
(20) Liu, Q.; Zhou, Y.; Ma, Y.; Zou, Z. *RSC Adv.* **2012**, *2*, 3247.
(21) Zhang, L.; Cao, X. F.; Chen, X. T.; Xue, Z. L. *CrystEngComm* **2011**, *13*, 2464.
(22) Guo, L.; Liu, C. M.; Wang, R. M.; Xu, H. B.; Wu, Z. Y.; Yang, S. *J. Am. Chem. Soc.* **2004**, *126*, 4530.
(23) Zhou, W.; Yao, M.; Guo, L.; Li, Y.; Li, J.; Yang, S. *J. Am. Chem. Soc.* **2009**, *131*, 2959.
(24) Beaulac, R.; Schneider, L.; Archer, P. I.; Bacher, G.; Gamelin, D. R. *Science* **2009**, *325*, 973.
(25) Yamanouchi, M.; Ieda, J.; Matsukura, F.; Barnes, S. E.; Maekawa, S.; Ohno, H. *Science* **2007**, *317*, 1726.
(26) Osada, M.; Ebina, Y.; Takada, K.; Sasaki, T. *Adv. Mater.* **2006**, *18*, 295.
(27) Huang, J. H.; Ding, K. N.; Wang, X. C.; Fu, X. Z. *Langmuir* **2009**, *25*, 8313.
(28) Dvoranova, D.; Brezova, V.; Mazur, M.; Malati, M. A. *Appl. Catal., B* **2002**, *37*, 91.
(29) Habisreutinger, S. N.; Schmidt-Mende, L.; Stolarczyk, J. K. *Angew. Chem., Int. Ed.* **2013**, *52*, 7372.
(30) Mori, K.; Yamashita, H.; Anpo, M. *RSC Adv.* **2012**, *2*, 3165.
(31) Roy, S. C.; Varghese, O. K.; Paulose, M.; Grimes, C. A. *ACS Nano* **2010**, *4*, 1259.
(32) Xi, G.; Ouyang, S.; Li, P.; Ye, J.; Ma, Q.; Su, N.; Bai, H.; Wang, C. *Angew. Chem., Int. Ed* **2012**, *51*, 2395.
(33) Yan, S. C.; Ouyang, S. X.; Gao, J.; Yang, M.; Feng, J. Y.; Fan, X. X.; Wan, L. J.; Li, Z. S.; Ye, J. H.; Zhou, Y.; Zou, Z. G. *Angew. Chem., Int. Ed.* **2010**, *49*, 6400.
(34) Tong, H.; Ouyang, S.; Bi, Y.; Umezawa, N.; Oshikiri, M.; Ye, J. *Adv. Mater.* **2012**, *24*, 229.
(35) Indrakanti, V. P.; Kubicki, J. D.; Schobert, H. H. *Energy Environ. Sci.* **2009**, *2*, 745.
(36) Xu, Y.; Schoonen, M. A. A. *Am. Mineral.* **2000**, *85*, 543.
(37) Butler, M. A.; Ginley, D. S. *J. Electrochem. Soc.* **1978**, *125*, 228.
(38) Yan, S.; Wang, J.; Gao, H.; Wang, N.; Yu, H.; Li, Z.; Zhou, Y.; Zou, Z. *Adv. Funct. Mater.* **2013**, *23*, 758.
(39) Tu, W. G.; Zhou, Y.; Liu, Q.; Tian, Z. P.; Gao, J.; Chen, X. Y.; Zhang, H. T.; Liu, J. G.; Zou, Z. G. *Adv. Funct. Mater.* **2012**, *22*, 1215.
(40) Liu, Q.; Zhou, Y.; Tian, Z.; Chen, X.; Gao, J.; Zou, Z. *J. Mater. Chem.* **2012**, *22*, 2033.